



High efficient degradation of levofloxacin by edge-selectively Fe@3D-WS₂: Self-renewing behavior and Degradation mechanism study

Fanqing Meng, Wei Ma*, Chunying Duan, Xin Liu, Zhen Chen, Moyan Wang, Jian Gao, Zhe Zhang

Department of Chemistry, Dalian University of Technology, Dalian, 116023, PR China



ARTICLE INFO

Keywords:
Tungsten disulfide
Ball milling
Active edges
Levofloxacin
Self-renewing

ABSTRACT

Two dimensional transition metal dichalcogenides as potential catalysts to solve energy and environmental crises have caused significant research interests in recent years. In this work, edge-selectively Fe@3D-WS₂ nanoflowers with the abundant single-layer were efficiently prepared by dry ball milling for levofloxacin (LEVO) elimination. Together with the advantages of the single-layer active edges and the stretch of W–S bond, the as-prepared Fe@3D-WS₂ showed the ultra-high degradation efficiency for LEVO under ball-milling condition. This high degradation activity was demonstrated to be originated from piezo-catalysis, rather than adsorption or thermocatalysis. In addition, the Fe@3D-WS₂ also showed an ultra-high reusability during the cyclic tests, which is due to its special “self-renewing” behavior under ball milling condition. The degradation efficiency of the Fe@3D-WS₂ still reached ~ 99% after ten cyclic tests. Both oxygen radicals ($\cdot\text{O}_2$, O_2^-) and $\cdot\text{OH}$ radicals were generated and took part in the LEVO degradation, while oxygen radicals were more contributed to the LEVO degradation. The present work not only provides an important insight for designing efficient catalysts, but also extends the possible application areas of ball milling technique.

1. Introduction

The piezoelectricity as one kind of physical characteristics has been widely applied in energy harvesting, acoustic imaging and non-destructive flaw detection field [1]. In the pursuit of these commercial applications, most piezoelectric studies were mainly aimed at the nano-generator, energy converter and self-powered nanosystem designing and fabricating [2–5]. Besides, recent studies have found that the piezoelectric materials also possessed a piezo-catalytic activity via a mechanical force activation attributed to their noncentrosymmetric structure [6]. For example, S.H. Lan et al. reported that the tetragonal BaTiO₃ nano/micrometer-sized particles could piezoelectrically degrade about 71.1% of 4Chlorophenol within 120 min [7]. Especially, J.M. Wu et al. discovered that few-layer MoS₂ nanoflowers could be used as efficient piezo-catalysts to remove organic dyes in a few minutes by imposing an ultrasonic wave [8]. Those discoveries provide a widespread option for the commercial applications of the piezo-catalysts [9].

For practical applications, excellent degradation activity and reusability are both important. However, due to the destroyed of the catalyst by mechanical force, the degradation efficiency of the catalyst was always decreased with the increasing of number of cyclic tests. So far, few approach has been applied to improve the repeatable ability of the

piezo-catalyst. Very recently, S. Masimukku et al. have found that the reusability of the catalyst could be improved by embedding the poly-dimethylsiloxane (PDMS) with catalyst, but the degradation efficiency of the modified catalyst was only 80% after ten cycles [10]. Therefore, it is needed to found an effective method for both improving the degradation activity and the repeatable ability of the piezo-catalyst.

Dry and wet ball milling as well-established and eco-friendly approaches were widely applied in the mechanochemical reactions and catalyst preparation [11–13]. Recently, the related research showed that the catalysts prepared via ball milling process exhibited higher thermodynamically stability and catalytic activity than others [14]. Moreover, new active edge sites and vacancies could be introduced following the ball milling process, which is essential to assure the repeatability and activity of the catalyst [15,16]. To the best of our knowledge, there has been no report published using ball milling method to synthesize the piezo-catalyst and provide vibration energy for piezo-degradation of contaminants [17,18].

In addition, related piezo-catalytic degradation articles mainly focused on the removal of dyes, and few non-dye pollutant has been studied [8,9]. Thus, the piezo-degradation mechanism of other organic pollutant is still unclear. Moreover, recent reports showed that a lot of antibiotic (such as LEVO) and their related compounds were observed in the natural water solution because they could not be totally absorbed

* Corresponding author.

E-mail address: chmaww@yahoo.com (W. Ma).

and completely used by humans' and animals' body [19–22]. Those residual contaminants in water could not only result in lots of adverse impacts on human health, but also restrict the water treatment efficiency [23,24]. In addition, the decomposed byproducts during the water treatment process were hardly decomposed by the traditional wastewater treatment plants [25]. It is needed to find a feasible method for efficient removal of LEVO and its related compounds in water solution.

In this work, we introduced a well-established and facile dry ball milling method to synthesize Fe@3D-WS₂ nanolayers with abundant active edges and vacancies. The surface morphology and crystal structure of the synthesized catalyst were characterized by SEM, XRD, TEM, XPS and Raman spectra. Then, the as-prepared Fe@3D-WS₂ was used as the potential piezo-catalyst for piezo-degradation of LEVO under ball-milling activation. The extremely long service life of Fe@3D-WS₂ was investigated by cyclic tests. The underlying mechanism of the high degradation efficiency and the "self-renewing" behavior of the Fe@3D-WS₂ under ball milling activation process were also studied. Finally, HRTEM, PFM and density functional theory (DFT) calculations were used to elaborate the enhancement mechanism of ferric atoms on vacancies generation and LEVO elimination. This work not only provides an efficient method for contaminant elimination, but also extends the possible application areas of ball milling.

2. Experimental section

2.1. Materials

Tungsten trioxide, hydrazoic acid sodium (NaN₃), LEVO and ferric trichloride were purchased from Sinopharm Chemical Reagent Co., Ltd. ethylenediaminetetraacetic acid disodium salt (EDTA), Tert-butyl-alcohol (TBA) and 1,4-benzoquinone (BQ) were purchased from Sigma-Aldrich (Shanghai, China). 5, 5-dimethyl-1-pyrroline-n-oxide (DMPO), Dimethyl sulfoxide (DMSO) and 2, 2, 6, 6-tetramethyl piperidine (TEMP) were purchased from Aladdin Chemical (Dalian, China). Titanium oxide (CAS:13463-67-7) with the anatase structure was purchased from Aladdin (Shanghai, China). All the reagents used in the study were analytical grade and all solutions were prepared with distilled (DI) water.

2.2. Methods

2.2.1. Preparation of 3D-WS₂

In a typical synthesis, the powder mixtures (W: S mole ratio of 1:15) of 2 g tungsten trioxide, 10 g thiocarbamide and 0.5 g sodium hydroxide were ball milled in air at 1000 rpm for 6 h. In the ball milling process, the zirconia balls with the diameter of 4 mm and a teflon reactor of 100 cm³ were used. Then, the powder product was heated at 450 °C for 2 h under N₂ solution. Finally, the product was washed several times with ethyl alcohol and DI water, and it was denoted as 3D-WS₂.

2.2.2. Preparation of Fe@3D-WS₂

Typically, 5 g as-prepared 3D-WS₂ and 0.5 g ferric trichloride was mixed in 100 mL DI water, accompanied by continuous magnetic stirring at room temperature for 3 h. Then, the suspension was collected by vacuum filtration (0.45 μm) and washed several times with DI water to obtained Fe@3D-WS₂ samples.

2.3. Characterization

X-ray diffraction (XRD) patterns of the prepared materials were recorded using Rigaku: D/Max 2400 with a GADDS powder X-ray diffractometer with a Cu Kα ($\lambda = 1.54 \text{ \AA}$) source at 40 kV and 40 mA over a range of 2θ angles from 10° to 80°. For electron microscopy measurements, the high resolution transmission electron microscopy (HRTEM, 200 keV, JEOL, JEM-2100f) and the scanning electron

microscopy (SEM, America, FEI: NOVA Nano SEM 450) were used. Fe 2p and W 4f components of the catalyst were identified using X-ray photoelectron spectroscopy (XPS, Thermo Fisher: ESCALAB 250Xi using mono Al Kα as the photoexcitation source). C 1s (C–C bond) was calibrated at 284.5 eV. Three-dimensional excitation-emission matrix fluorescence spectra (3D EEMs) and PL spectra were recorded on a Hitachi fluorescence spectrophotometer (FL4500, Japan). Raman spectroscopy (inVia, Renishaw) with a solid-state laser (wavelength ~ 532 nm) was used to investigate the synthesized 3D-WS₂. The electron spin resonance (ESR) signals of radicals spin-trapped by spin-trapped reagent DMSO, DMPO and TEMP, were examined on a Bruker A200 spectrometer under visible light irradiation ($k > 420 \text{ nm}$). AFM and the piezoresponsive force microscopy (Bruker, BioScope, PFM) measurements were carried out with a digital instruments nanoscope III scanning probe microscope (Dimension ICON). The instrument was equipped with silicon tip and operated in tapping mode.

2.4. Piezo-catalytic activity evaluation

The degradation activities of the samples were evaluated by piezo-catalytic degradation of LEVO (25 mg/L) under the mechanical force in the dark environment. For comparison, the degradation efficiency of LEVO by using non-piezoelectric material TiO₂ were also investigated. Typically, 20.0 mg catalyst samples (Fe@3D-WS₂, 3D-WS₂, the commercial WS₂ and TiO₂) and 40 mL LEVO were mixed in a 100 mL teflon reactor with appropriate dose of zirconia ball (4 mm). The ball mill reactor (1000 rpm) was used as a mechanical force under dark environment. Then, the solution was filtrated by ultrafiltrate membrane (0.45 μm) and the residual LEVO was measured by High Performance Liquid Chromatography (HPLC) (Agilent HP1100 G1312 A) [19]. Determination of the electro-degradation intermediates of LEVO were carried out on a Daojin LC-MS system (LCMS-2010 A, Japan). Concentration of NO₂⁻ and NO₃⁻ generated from LEVO degradation process were analyzed by using a Dionex Ion Chromatography (DIONEX ICS-5000, USA). The concentration of NH₄⁺ was measured (as NH₃-N) using UV-vis spectrophotometer (D2100, China). Concentration of generated N₂ was analyzed by using Gas Chromatography (GC Tianmei 7900, China). Detailed conditions applied in HPLC, LC-MS, IC, UV-vis spectrophotometer and GC were shown in supporting information.

3. Results and discussion

3.1. Composition and morphology

In order to study the chemical composition of the as-prepared catalysts, the element distributions of W, S and Fe in the catalysts were investigated by an X-ray fluorescence spectrometer (EDX-7000, Daojin). It can be seen from the EDX analysis (Table S1) that the W:S ratio of the as-prepared 3D-WS₂ was nearly 1: 2, confirming that the synthetic strategy was successful. Moreover, the concentration of Fe element in the Fe@3D-WS₂ was found to be 4.12 wt%, which suggested that Fe atoms were successfully introduced. It is worth noting that W:S ratio in the as-prepared Fe@3D-WS₂ was slightly smaller than the stoichiometric ratio of 3D-WS₂, confirming that the S atoms was bonded with the Fe atoms during the dipping process [9].

The morphology, structure, and the chemical states information of the prepared Fe@3D-WS₂, 3D-WS₂ and the commercial WS₂ were analyzed by SEM, TEM, XRD and Raman spectra. SEM and TEM images of the as-prepared materials were shown in Fig. 1 and Fig. S1. Compare with the commercial WS₂ (Fig. S1 (a) and (c)), the 3D-WS₂ (Fig. S1 (b)) showed the special nanoflowers structure with obviously thinner thickness. More uniform nano-petals with average sizes of 0.5–2 μm were observed when Fe atoms were loaded, as shown in Fig. 1(a) and (b). Consistent with the results of the SEM images, TEM image in Fig. 1(c) further showed that the well-dispersed Fe@3D-WS₂ nanoflowers was composed of few-layered WS₂. Moreover, the energy

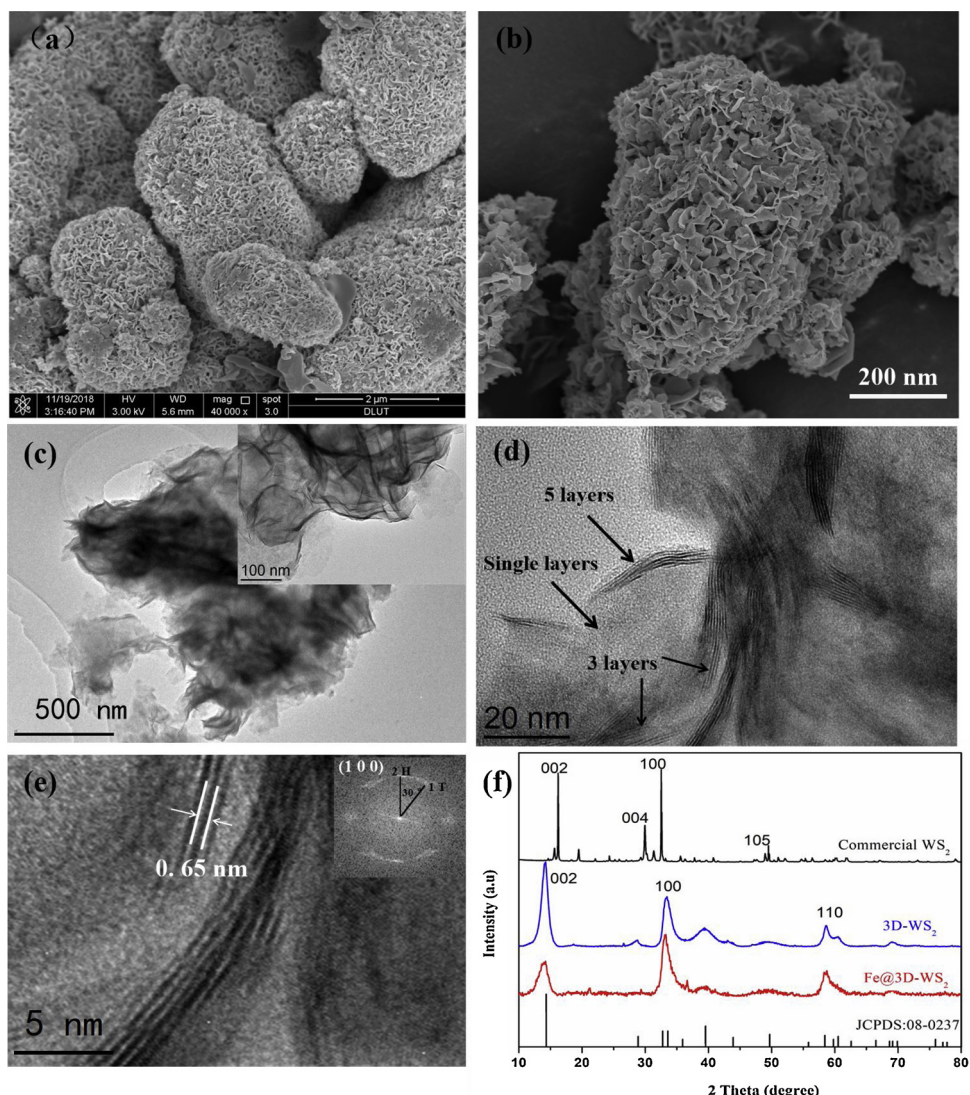


Fig. 1. (a) and (b) The SEM image the as-prepared Fe@3D-WS₂. (c) TEM images of the morphology of Fe@3D-WS₂. (d) HRTEM of layer structure of Fe@3D-WS₂. (e) The lattice spacing between the two layers and the fast Fourier transform (FFT) patterns of Fe@3D-WS₂. (f) XRD patterns of the commercial WS₂, 3D-WS₂ and Fe@3D-WS₂.

dispersive x-ray spectroscopy (EDX) mapping images (Fig. S2) of Fe@3D-WS₂ obviously revealed the uniform distribution of the iron, tungsten and sulphur, which indicated that Fe atoms were well distributed in the as-prepared Fe@3D-WS₂ [10]. To elucidate the layers information of the as-prepared WS₂ materials, the HRTEM images were also studied. As presented in Fig. 1(d) and (e), the distinctly active edge sites of the Fe@3D-WS₂ nanoflowers was formed by few-layered WS₂, which was between single to five layers. Fig. 1(e) also showed that the interlayer spacing of two single layers was \approx 0.65 nm. The fast Fourier transform (FFT) pattern in the inset of Fig. 1(e) demonstrated that the preferential growth plane of the active edges was (1 0 0) plane. For the 3D-WS₂, typical nanoflowers structure with 5–8 layers was observed (Fig. S1(d) and (f)). In addition, typically hexagonal spots with six-fold symmetry and additional twisted hexagonal spots were observed in Fe@3D-WS₂ and 3D-WS₂. As shown in the inset of Fig. 1 (e) and Fig. S1 (f), the angle between 2H and 1T phases was 30° angular, indicating that the prepared Fe@3D-WS₂ and 3D-WS₂ were both consisted of 2H and 1T phases of WS₂, in which the contribution of 1T phase WS₂ was more dominant [26]. In contrast, for the commercial WS₂ (Fig. S1(e)), no angle was observed in the diffraction spots, suggesting that the biggest contribution was from the 2H phase [27].

As shown in XRD patterns (Fig. 1(f)), all of the prepared Fe@3D-

WS₂, 3D-WS₂, and the commercial WS₂ agreed well with WS₂ structure (JCDPS NO.08-0237). Compared with the commercial WS₂ sheets, the (002) peak of the as-prepared Fe@3D-WS₂ and 3D-WS₂ appeared at a lower 2θ angle, which suggested that more 1T metallic phases were formed in the as-prepared materials [28]. More especially, it is noticed that the preferred orientation of the as-prepared 3D-WS₂ was changed when introducing of Fe atoms. As shown in Table 1, the relative intensity of $I_{(0\ 0\ 2)} / I_{(1\ 0\ 0)}$ for the Fe@3D-WS₂ was 0.59, which implied that Fe@3D-WS₂ has an obviously preferred orientation along with (1 0 0) plane. In addition, a broader (002) plane with a much lower intensity was observed in the as-prepared Fe@3D-WS₂ compared with other catalyst, which indicated that the Fe@3D-WS₂ possessed a few-layered

Table 1
Summarization of the structure information of prepared materials.

Materials	$I_{(0\ 0\ 2)} / I_{(1\ 0\ 0)}$	Preferred orientation plane
Commercial WS ₂	0.96	–
3D-WS ₂	1.64	(0 0 2)
3D-WS ₂ used for ten cycles	1.01	–
Fe@3D-WS ₂	0.59	(1 0 0)
Fe@3D-WS ₂ used for ten cycles	0.54	(1 0 0)

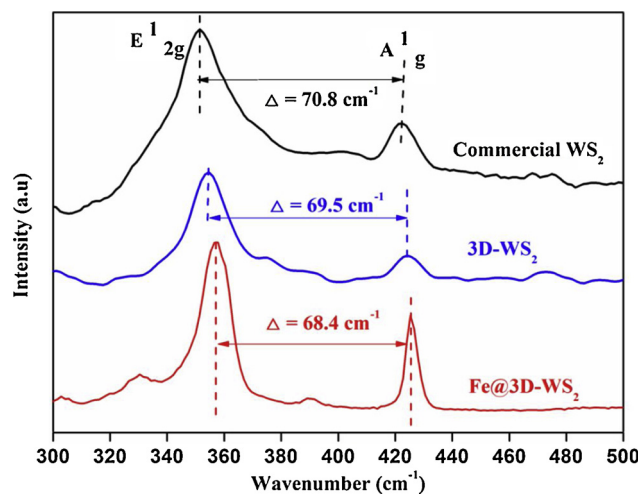


Fig. 2. The comparison of the Raman spectra for the commercial WS_2 , 3D- WS_2 and $\text{Fe}@\text{3D-WS}_2$.

structure [29,30].

Raman spectra of various WS_2 samples was analyzed and the results were presented in Fig. 2. Two pronounced peaks at 352.1 cm^{-1} and 422.9 cm^{-1} were observed in the commercial WS_2 , which were corresponding to the in-plane vibration (E_g^1) and the out-of-plane mode (A_g^1), respectively [31]. The peak spacing between of the A_g^1 peak and E_g^1 peak was found to be sensitive to the number of the WS_2 layers [32]. The lower peak spacing of the 3D- WS_2 (69.5 cm^{-1}) implied the reducing of the WS_2 layers. Additionally, an obvious red-shift of A_g^1 peak was observed in 3D- WS_2 , suggested that the prepared 3D- WS_2 was few-layered structure [33]. Interestingly, for $\text{Fe}@\text{3D-WS}_2$ samples, a much greater red-shift of A_g^1 peak and reduction of peak spacing were observed. Those changes indicated that the $\text{Fe}@\text{3D-WS}_2$ possessed the least layered structure compared with the commercial WS_2 and 3D- WS_2 , which is consistent with HRTEM results.

In order to obtain the information of the polymorphs (2H and 1T) and the chemical states of the as-prepared catalysts, the XPS spectroscopy of the $\text{Fe}@\text{3D-WS}_2$, 3D- WS_2 and the commercial WS_2 were all investigated. As shown in Fig. 3, the W 4f spectra of the as-prepared 3D- WS_2 was quite different to those of the commercial WS_2 . According to analysis of the W 4f spectra (Fig. 3(b)) of the commercial WS_2 , most of the W signals arose at 33, 35, 36.7 eV and 38.9 eV, indicating the commercial WS_2 was more dominated by 2H-phase. For the as-prepared 3D- WS_2 (Fig. 3(c)), more prominent peaks were observed at 32 eV and 34 eV, which were ascribed to the 1T metallic phase. When Fe atom was loaded (Fig. 3(d)), the proportion of 1T metallic phase was increased from 42.4% to 52.5%, which demonstrated that the polymorph of the as-prepared $\text{Fe}@\text{3D-WS}_2$ was 1T metallic phase. Furthermore, the 1T metallic phase revealed the higher catalytic and electronic properties than that of the 2H phase [9,34–36]. The corresponding Fe 2p peaks of the as-prepared materials were also studied and the results were given in Fig. S3. According to analysis of the Fe 2p spectra, most of the Fe (III) signals arose at 724.9 eV and 711.5 eV, which indicated that Fe^{3+} was the main ingredient of the loaded iron ions.

3.2. Piezoelectric properties

To explore the piezoelectricity of the as-prepared $\text{Fe}@\text{3D-WS}_2$ and 3D- WS_2 , the AFM and the piezoresponse force microscopy (PFM) of the materials were investigated. Fig. S4 (a) and Fig. 4(a, b) presented the three-dimensional images of the commercial WS_2 , 3D- WS_2 and $\text{Fe}@\text{3D-WS}_2$, which represented the quantitative height signal and the detail surfaces of the prepared materials, respectively. Compared with the commercial WS_2 , the as-prepared 3D- WS_2 and $\text{Fe}@\text{3D-WS}_2$ revealed fewer layers in height, which is consistent with the HRTEM images. In

point of fact, a conductive tip was brought into contact with the samples by applying the a.c bias along the in-plane direction, and the out of plane piezoelectric response signals was extracted from the z-deflection [9]. As shown in Figs. 4(c, d) and S4(b), a highest piezoelectric response signal 62.9 mV was extracted from the $\text{Fe}@\text{3D-WS}_2$, which was distributed uniformly around the $\text{Fe}@\text{3D-WS}_2$ planes. Those results could explain why the $\text{Fe}@\text{3D-WS}_2$ revealed the highest piezo-degradation activity in contrast to the other catalysts.

In order to understand the effect of the loaded Fe atoms on the structure and piezoelectric property of the WS_2 nanolayer, the density functional theory (DFT) calculations of the bare WS_2 nanolayer and Fe loaded WS_2 nanolayer were both studied. On the T_w , H and T_s adsorption sites (Fig. S5), the adsorbed Fe atom could bond to the neighboring S atom, and the length of the Fe-S bond was 0.261, 0.255 and 0.246 nm, respectively (Table 2). Furthermore, the most stable adsorption site for Fe atom on WS_2 nanolayer directly lied on above the W atom (T_w) and the atomic adsorption energy was ca. 1.84 eV. The interaction between Fe atom and substrate atoms could weak the nearest W-S bonds, and the length of the W-S bond was increased from 0.242 to 0.261 nm. This weakness of the W-S bond could significantly improve the noncentrosymmetric property of the WS_2 nanolayer, which benefited to the generation of active vacancies and the separation of the electron and hole [37,38]. Moreover, the band-structure calculations in Fig. 5 revealed that the Fe loaded WS_2 showed a lower band gap (0.94 eV) than the pure WS_2 (1.93 eV), which is efficient to reduce the separation resistance of the electron and hole [37,38]. These calculations can explain how the $\text{Fe}@\text{3D-WS}_2$ layer possessed a larger piezoelectric response than the bare 3D- WS_2 layer.

3.3. Piezodegradation efficiency

To explore the piezo-degradation activity of the prepared piezocatalysts on degradation of LEVO, ball-milling activation was used as the vibration power to trigger the piezo-catalytic degradation experiments. Fig. 6(a) presented the degradation efficiencies of LEVO for the piezo-catalytic experiments within 12 min. In the commercial WS_2 piezo-catalytic solution, only 18% LEVO was decomposed. When using the as-prepared 3D- WS_2 as piezo-catalyst, the degradation ratio for LEVO was slightly improved and reached 63% within 12 min. Surprisingly, nearly all of LEVO were decomposed in the $\text{Fe}@\text{3D-WS}_2$ piezo-catalytic solution, and the degradation yield reached 99.6% when extending the reaction time to 12 min. As represented in Fig. 6(b), the good linear fit ($R^2 = 0.992\sim0.996$) of the degradation results indicated that degradation of LEVO on as-prepared materials were all followed by pseudo-first order kinetics. In addition, there was a 3-fold increase in degradation yield when $\text{Fe}@\text{3D-WS}_2$ was used as piezo-catalyst compared to that when 3D- WS_2 was used. On the contrary, another nonpiezoelectric material TiO_2 just removed 8% LEVO within 12 min under the same experimental conditions. Those results demonstrated that the degradation of LEVO was mainly attributed to the piezocatalysis property of the as-prepared catalysts.

Besides, in order to compare the piezo-catalytic activity of prepared $\text{Fe}@\text{3D-WS}_2$ with the reported materials, the piezo-catalytic degradation experiments of Rhodamine dye (1000 ppm, 20 mL) were conducted under ultrasonic vibration in the presence of 0.01 g of catalyst. As shown in Fig. S6 (a), the degradation ratio of the Rh-B dye reached 98% within 30 s, which is more efficient than that of the reported WS_2 nanoflowers [8,9].

It is noticed that the temperature is raised easily in the ball milling process. Thus, to exclude the impact on the degradation of LEVO caused by the temperature raising, the thermocatalytic degradation experiment was also investigated. In the thermocatalytic degradation reaction, 20.0 mg catalyst samples and 40 mL of LEVO (25 mg/L) were mixed in a 100 mL constant temperature reactor which was kept under constant stirring in dark for 15 min. As presented in Fig. S6 (b), the removal rate of LEVO slightly increased with the increasing of the reaction

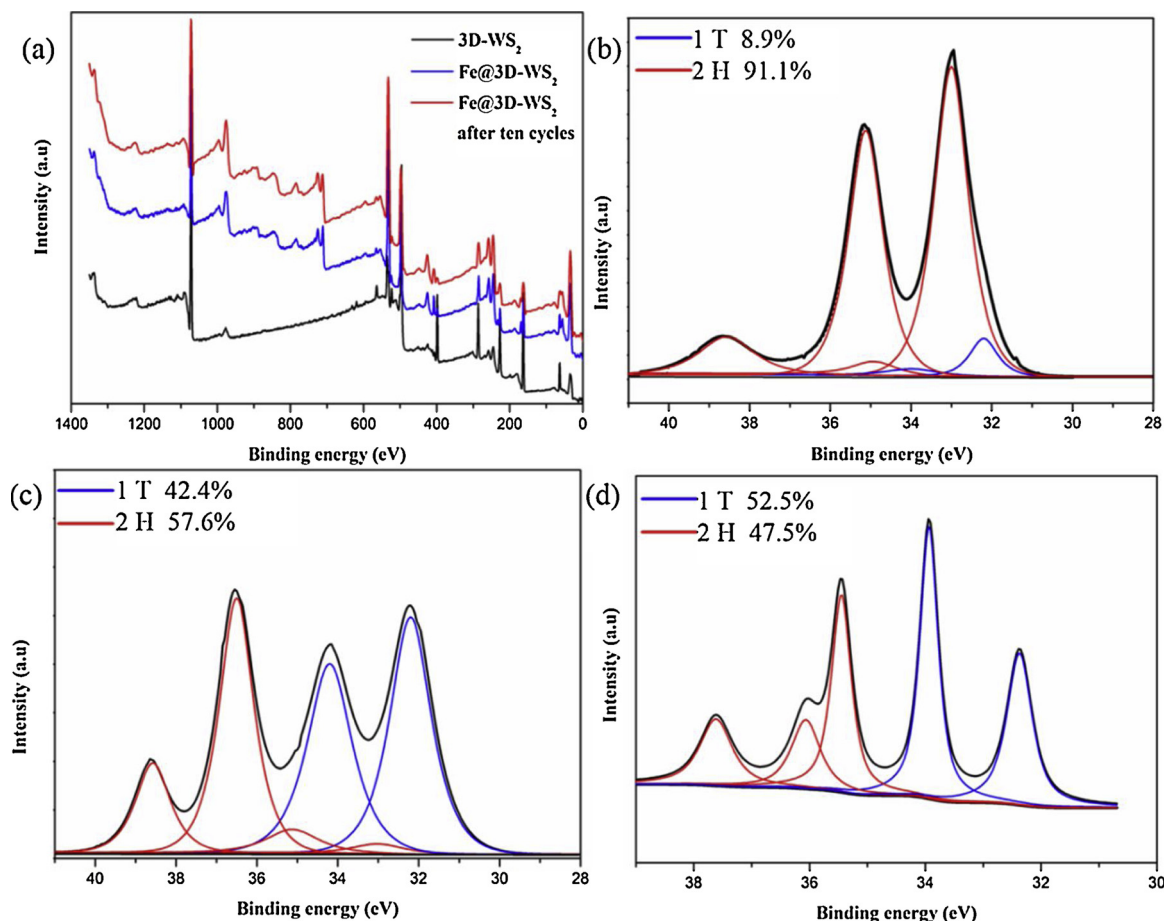


Fig. 3. (a) XPS spectra of the prepare catalysts and high-resolution XPS spectra of W 4f of (b) the commercial WS₂, (c) 3D-WS₂ and (d) Fe@3D-WS₂.

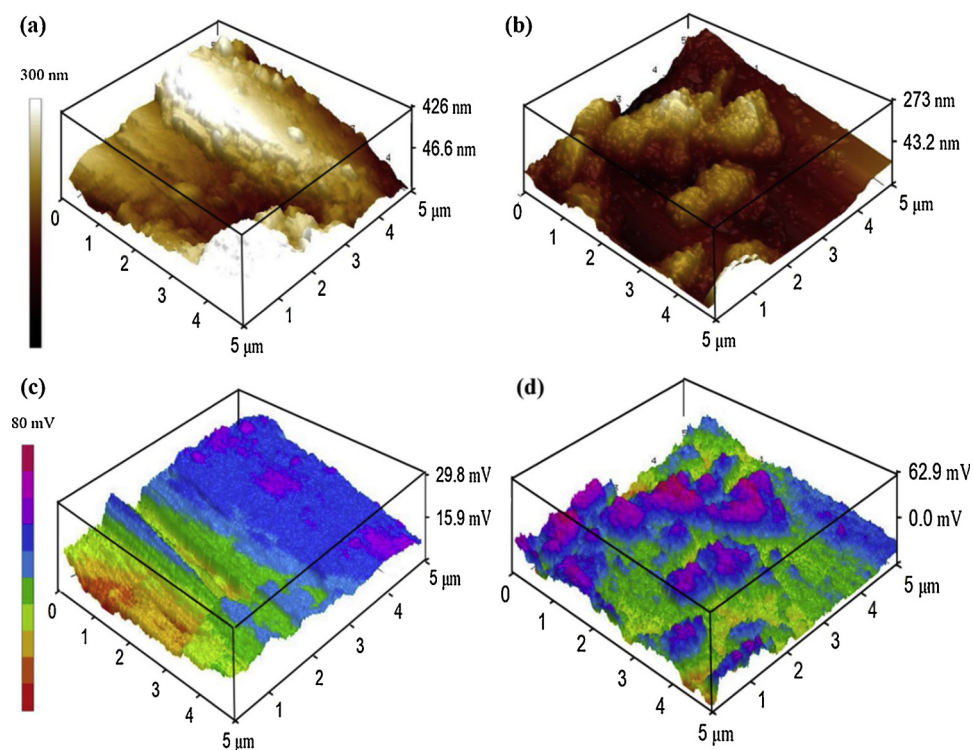


Fig. 4. The 3D deflection images of (a) 3D-WS₂ and (b) Fe@3D-WS₂. The output piezoelectric potential responsive images of (c) 3D-WS₂ and (d) Fe@3D-WS₂.

Table 2Adsorption energy and bond lengths of W–S and Fe–W in the Fe loaded WS₂.

Adsorption sites	<i>E_{ads}</i> /eV	<i>d_{W-S}</i> /nm	<i>d_{Fe-S}</i> /nm
Bare WS ₂	–	0.242	–
Fe on WS ₂ (T _W)	1.92	0.261	0.219
Fe on WS ₂ (H)	1.48	0.255	0.215
Fe on WS ₂ (T _S)	0.83	0.246	0.232

temperature, but this improvement was quite small, just 23.6% LEVO was decomposed when the thermocatalytic temperature is 323 K. In the piezo-catalytic test, after 12-minutes ball-milling activation, the solution temperature was increased from 295.6 K to 309.6 K within the 12 min. However, as shown in red bar of Fig. S6 (b), only 8.6% LEVO was decomposed when the thermocatalytic temperature is 309.6 K, which indicated that the thermocatalysis caused by the increase temperature was not the key factor in the piezo-degradation of LEVO. Additionally, adsorption performance as another key factor to influence the degradation activity was also studied and the results were given in Fig. 6 (c). It could be seen that all as-prepared catalysts exhibited a very low adsorption performance on LEVO. Although, the adsorption of LEVO could increase by introducing ferric ions, but the improvement was quite small, just 16% LEVO was adsorbed within 12 min. Additionally, the PL spectra in Fig. S7 (a) revealed that a strong PL emission peak was observed at 440 nm after soaked the Fe@3D-WS₂ into LEVO solution for 12 min, which is attributed to the special fluorescence characteristic of the adsorbed LEVO. After 12-minutes piezo-degradation, typically PL emission peak of LEVO was disappeared, and showed a similar spectra as bare Fe@3D-WS₂. The results above reconfirmed that the piezo-catalytic reaction under ball-milling treatment was the key factor in piezo-degradation of LEVO.

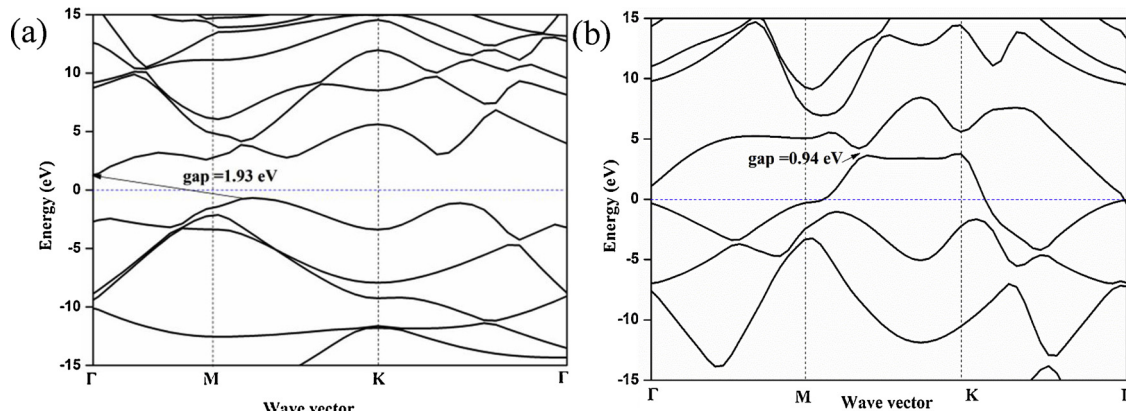
Good stability and reusability of catalysts are beneficial to their engineering applications. The reusability of the Fe@3D-WS₂ was investigated by ten cyclic piezo-degradation tests. Particularly, as shown in Figs. 6(d) and S6 (c), the piezo-degradation activity of the Fe@3D-WS₂ was very stable for each cyclic piezo-degradation test. As shown in Table S2, the apparent rate constant (*k*) values of LEVO degradation process were increased with the increase of cyclic tests, confirming the continual “self-renewing” behavior of Fe@3D-WS₂ during ball milling activation. In addition, the stability of Fe@3D-WS₂ was investigated after ten cycles. As represented in Fig. S7 (b), only Fe ions were detected in the aqueous after ten cycles and the concentration of the total released iron was lower than 0.1 mg/L, indicating the good mechanical stability of the Fe@3D-WS₂. To further understand the ball milling activation effect on the durability of catalyst, the repeated piezo-degradation activity of the Fe@3D-WS₂ under the ultrasonic-wave (40 kHz; 100 W) in dark was also analyzed. As shown in Fig. S6 (d), in the first cyclic test, the degradation efficiency of LEVO was 90% within

15 min and the degradation efficiency was slightly decreased with the increasing of the cycle times. When increasing the number of cyclic tests to five, the degradation ratio of LEVO was rapidly decreased to 74%. The above results confirmed that the wet ball milling activation process could significantly improve the durability and stability of catalysts.

In order to further understand the “self-renewing” behavior of the Fe@3D-WS₂ in the cyclic tests, the structure and surface morphology changes of Fe@3D-WS₂ during ten cyclic tests were thoroughly analyzed. The XRD patterns of the as-prepared samples during ten cyclic tests (“used”) were presented in Fig. 7(d) and the relative intensity information was summarized in Table 1. Compared with the virginal catalysts, the relative intensity of $I_{(0\ 0\ 2)} / I_{(1\ 0\ 0)}$ for the “used” 3D-WS₂ samples was obviously decreased, which implied that more (1 0 0) planes were exposed after wet ball milling activation. For the “used” Fe@3D-WS₂, no obviously change in peak intensity was observed in the XRD patterns, which suggested that the as-prepared Fe@3D-WS₂ had good structural stability. Besides, XPS spectroscopy of the “used” Fe@3D-WS₂ (Fig. S3) further revealed that more 1 T metallic phases were observed after ten cyclic tests, which is important to ensure the excellent catalytic and electronic properties. Furthermore, SEM image and TEM image revealed that the fewer layers and better dispersion were observed in the “used” Fe@3D-WS₂ compared with the virginal one, as shown in Fig. 7(a–c). Specifically, more active edges sites (single layer) were exposed in the “used” Fe@3D-WS₂ after 120-minutes ball milling (ten cycles). Meanwhile, it is well-known that the single layered WS₂ was more efficient to generate the highest piezoelectric response compared with the multilayer one [8]. Thus, those results can explain why the Fe@3D-WS₂ showed ultra-high degradation efficiency and the extremely long service life in cyclic ball milling tests.

3.4. Degradation path

3D EEM fluorescence spectra is a sensitive technique to determine the degradation activity and the degree of organic pollution. In order to understand the degradation process of LEVO better, the 3D EEM fluorescence spectra of the LEVO samples under different reaction time by using the Fe@3D-WS₂ as the catalyst was analyzed. As shown in Fig. 8, two main peaks could be identified as the acid-like substances of LEVO, which were located at $E_x/E_m = 300\text{--}360 / 400\text{--}550$ nm (peak A) and $E_x/E_m = 220\text{--}270 / 400\text{--}550$ nm (peak B), respectively [39]. The intensity of fluorescence peak A and peak B decreased gradually when extending the reaction time to 4 min, and a new peak appeared at $E_x/E_m = 270\text{--}290 / 425\text{--}500$ nm (peak C), which suggested that the conjugated heterocycle structure of LEVO was destroyed. Then, the intensity of peak A and B were further decreased with the extension of the reaction time to 10 min, and two new peaks appeared at $E_x/E_m = 240\text{--}260 / 425\text{--}480$ nm (peak D) and $E_x/E_m = 220\text{--}230 / 425\text{--}480$ nm (peak E).

Fig. 5. Band structure of (a) pure WS₂ and (b) Fe modified WS₂.

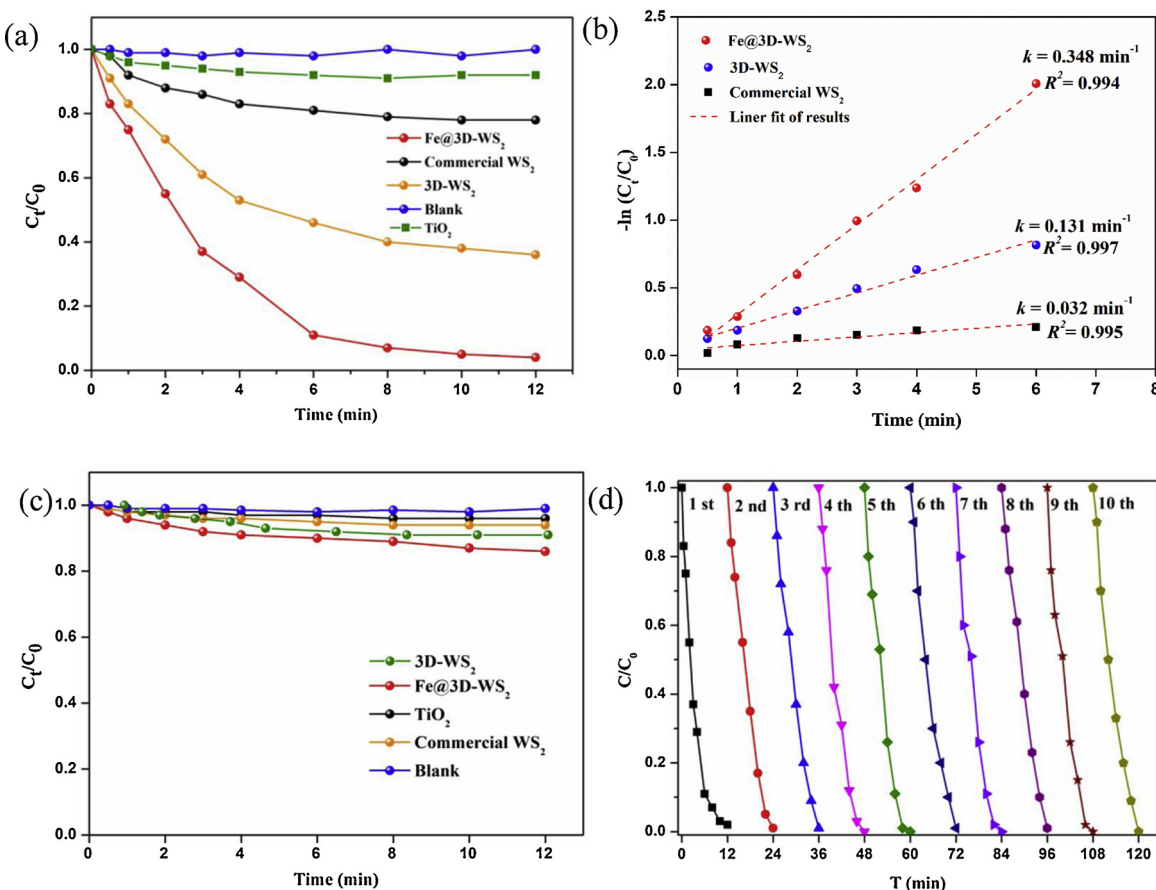


Fig. 6. (a) and (b) Degradation activity of LEVO using the commercial WS₂, TiO₂, 3D-WS₂ and Fe@3D-WS₂. (c) Adsorption capacity of the commercial WS₂, TiO₂, 3D-WS₂ and Fe@3D-WS₂ on LEVO without mechanical vibration. (d) Cyclic degradation tests of Fe@3D-WS₂.

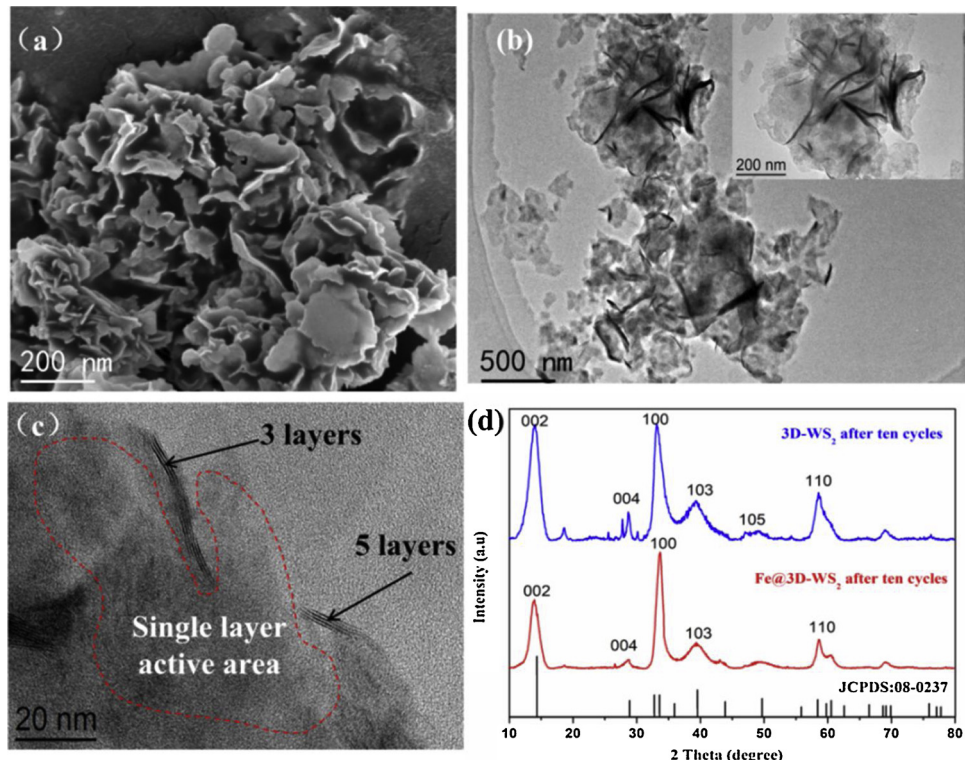


Fig. 7. (a) The SEM image of the Fe@3D-WS₂ after ten cycles. (b) TEM images of the morphology of Fe@3D-WS₂ after ten cycles. (c) HRTEM of layer structure of Fe@3D-WS₂. (d) XRD patterns of the “used” 3D-WS₂ and Fe@3D-WS₂.

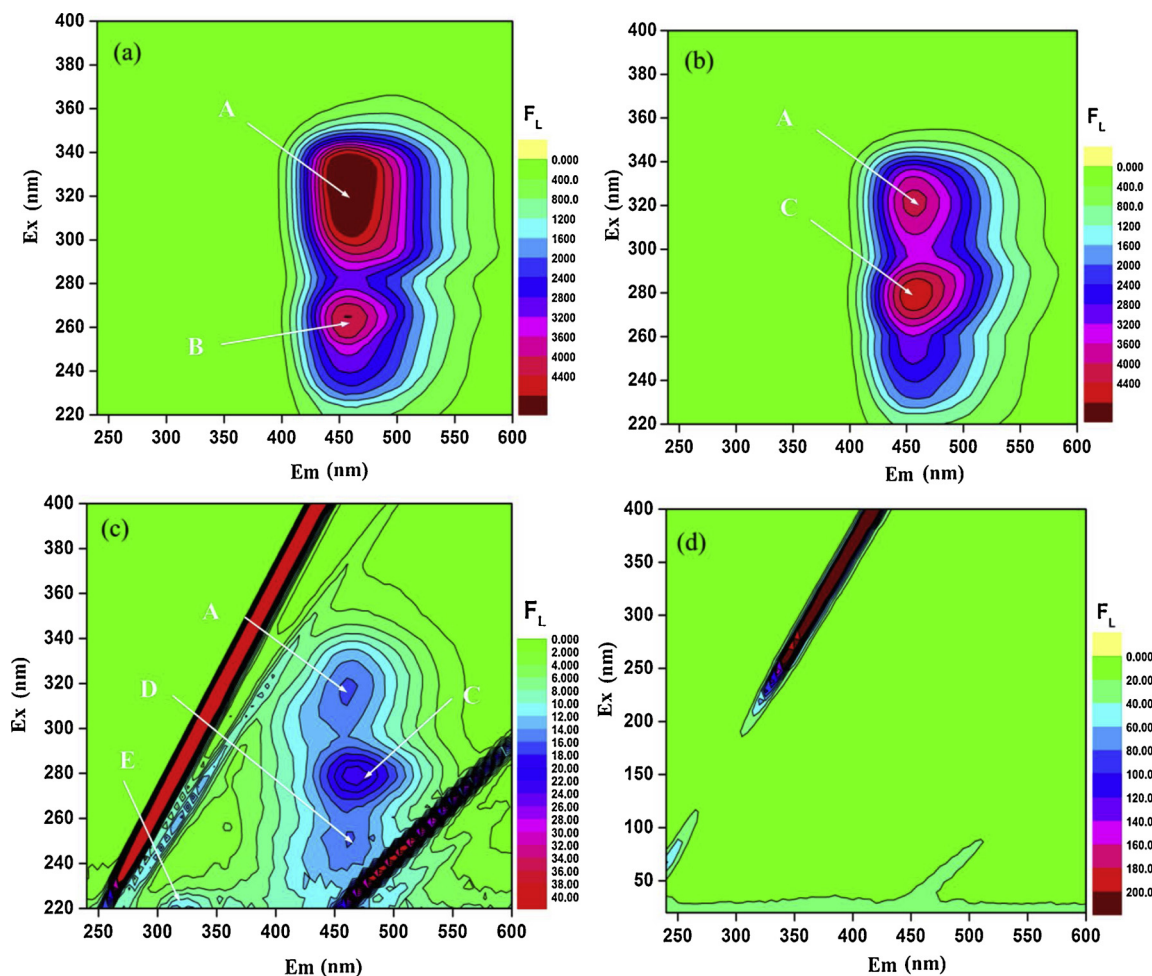


Fig. 8. 3D EEMs of the LEVO solution after piezo-catalytic degradation of (a) 0, (b) 4, (c) 10 and (d) 12 min by Fe@3D-WS₂.

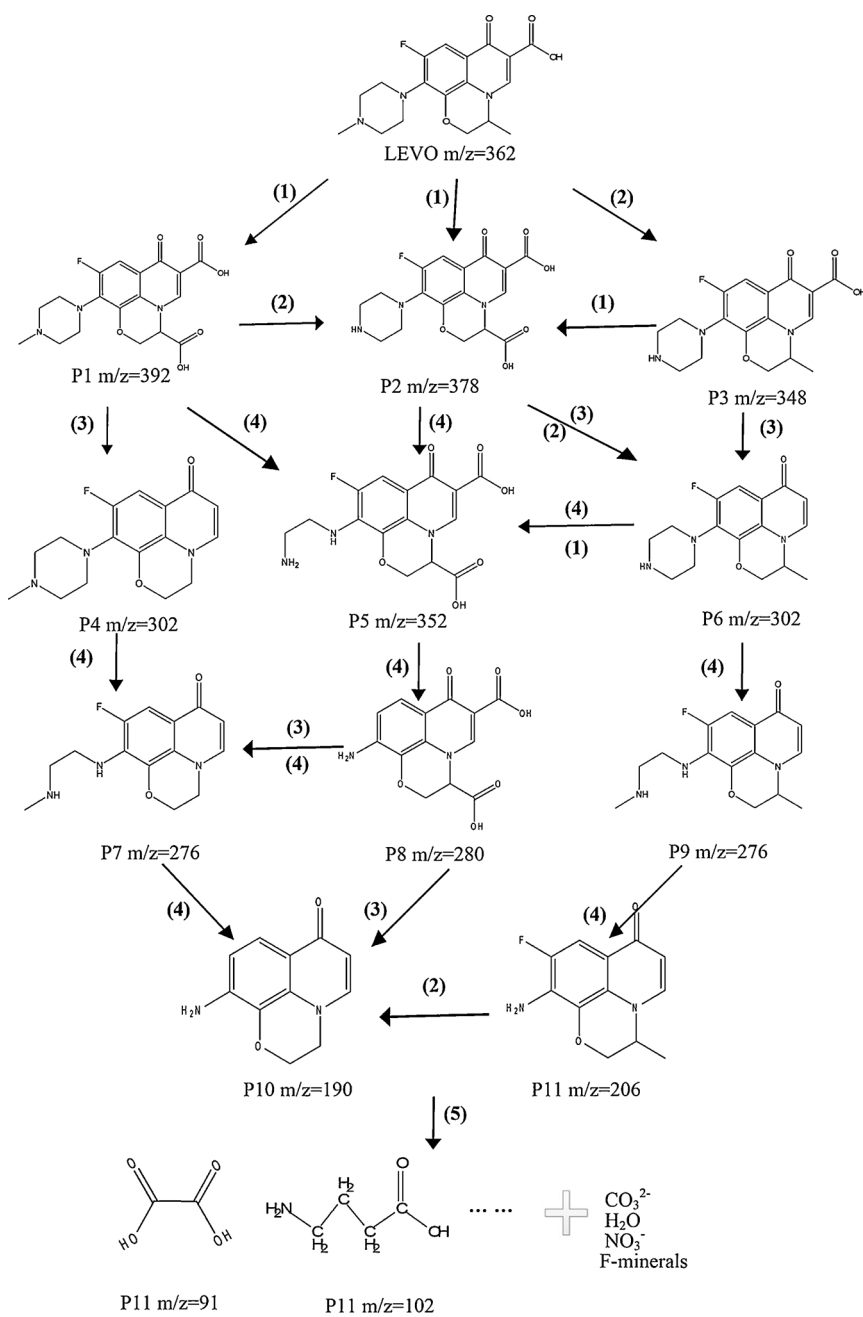
300–350 nm (peak E), indicating that the conjugated heterocycle structure of LEVO could be further destroyed and some intermediates were generated. When extending the reaction time to 12 min, all the fluorescence peaks disappeared, suggesting that both of LEVO and its intermediates were totally decomposed into non-fluorescent molecules after piezo-degradation process.

In order to further understand LEVO piezo-degradation process, LC-MS was also conducted. Based on the LC-MS results and 3D EEM fluorescence spectra, the main pathway of piezo-degradation for LEVO could be described as Fig. 9. It can be concluded that the piezo-degradation of LEVO by Fe@3D-WS₂ was mainly through five possible degradation pathways, which include carboxylation, de-carboxylation, de-methylation, de-piperazinylation and ring opening process [40]. As the data showed, the ion at *m/z* 362 represented LEVO which is consistent with its molecular weight. Firstly, three main intermediates P1 (*m/z* 392), P2 (*m/z* 378) and P3 (*m/z* 348) were generated after carboxylation and de-methylation process. Then, those intermediates were further degraded into P4 (*m/z* 302), P5 (*m/z* 352) and P6 (*m/z* 302) by the following de-piperazinylation and decarboxylation process. Next, those three intermediate products were further decomposed into P7 (*m/z* 276), P8 (*m/z* 280), and P9 (*m/z* 276). After that, all intermediates were converted into lower molecular intermediates P10 (*m/z* 190) and P11 (*m/z* 206). Finally, all the generated intermediates will be degraded to smaller molecule compounds (such as P12 (*m/z* 190) and P13 (*m/z* 102), CO₂, H₂O, smaller N-minerals and F-minerals, which agree with the 3D EEM fluorescence spectra results. Furthermore, the N-minerals of LEVO degradation process were also studied. As presented in Fig. S8, only NO₃⁻, NH₄⁺ and NO₂⁻ were

detected in LEVO piezo-degradation process. At the first 2 min, no N-minerals was detected because there is no de-piperazinylation reaction occurred in the beginning of the piezo-degradation process, which is consistent with the LC-MS result. When extending the reaction time to 8 min, the formation of NH₄⁺ was rapid and achieved maximum release of 2.4 mg/L. At the same time, about 6.2 mg/L NO₃⁻ and a small amount of NO₂⁻ were also generated. Then, the concentration level of NH₄⁺ and NO₂⁻ was significantly decreased, and most of the N-minerals were transformed into NO₃⁻ when extending the reaction time to 12 min. It might be because the generated NH₄⁺ and NO₂⁻ were further oxidized by the free radicals. Overall, in the piezo-degradation of LEVO, the formation of N₂ was marginal as compared to forms of inorganic nitrogen, and NO₃⁻ was the main inorganic nitrogen product.

3.5. Mechanism of LEVO degradation

Previous research has suggested that there are various active species generated and took part in the piezo-degradation process, such as h⁺, ·OH, O₂⁻, ¹O₂ and H₂O₂. Therefore, in order to investigate the formation of those reactive radicals in the Fe@3D-WS₂ piezo-catalytic process, the necessary radical quenching experiments were utilized. EDTA, TBA, BQ and NaN₃ were used as selective scavengers to distinguish the contribution of h⁺, ·OH, O₂⁻ and ¹O₂, respectively [41,42]. As presented in Fig. S9, no significant change in LEVO degradation was observed in the condition of 20 mM EDTA, suggesting that there are fewer h⁺ generated following the piezo-degradation process. Meanwhile, when 20 mM BQ and TBA was added, the degradation yield of LEVO were slightly declined 11.2% and 27.3%, respectively. This result



(1) Carboxylation; (2) De-methylation; (3) De-carboxylation; (4) De-piperazinylation; (5) Ring opening

Fig. 9. A possible degradation path of the LEVO piezo-catalytic degradation by Fe@3D-WS₂.

indicated that both O_2^- and $\cdot\text{OH}$ were generated and took part in the LEVO degradation. More importantly, when NaN_3 (20 mM) was introduced, the degradation yield of LEVO was significantly decreased from 99.6% to 56.7%, confirmed that a large number of ${}^1\text{O}_2$ were generated in the LEVO degradation process. Besides, the concentration of generated H_2O_2 was analyzed by a typical spectrophotometrical method [7]. When 20 mM Terephthalic acid as non-fluorescent molecules were added, no typically fluorescence spectra was observed (not given), implying almost no H_2O_2 was generated in LEVO piezo-degradation solution. This result also indicated that Fenton-like reaction was uninvolved in the degradation of LEVO, although Fe atoms were loaded. This might be because the loaded Fe atom was almost all Fe (III), which is consistent with the XPS results.

The generation of those radicals was further investigated by ESR technique by using DMPO, TEMP and DMSO as the capture agents. As

displayed in Fig. 10(a), the DMPO–OH signals with four lines (1:2:2:1) was obtained in the first five minutes. Then, the intensity of the DMPO–OH signals was decreased with increasing the reaction time to 10 min, which was due to DMPO was fully adsorbed by the generated hydroxyl radicals. It is implied that the concentration of generated hydroxyl radicals was very low, which agree well with the radical quenching results. For comparison, Fig. 10(b) displayed the intensity of 1:1:1 signal characteristic of ${}^1\text{O}_2$ radicals trapped by TEMP [43]. Unlike DMPO–OH signals, the ${}^1\text{O}_2$ radical signals were increased with the increasing reaction time. Meanwhile, when DMPO/DMSO was introduced, typically O_2^- signals were observed in ESR spectra (Fig. 10(c)), denoting that O_2^- occurred in the piezo-catalytic system as well. Those results demonstrated that both of the oxygen radicals (${}^1\text{O}_2$ and O_2^-) and the hydroxyl radicals were generated and took part in the LEVO degradation process, while the contribution of oxygen

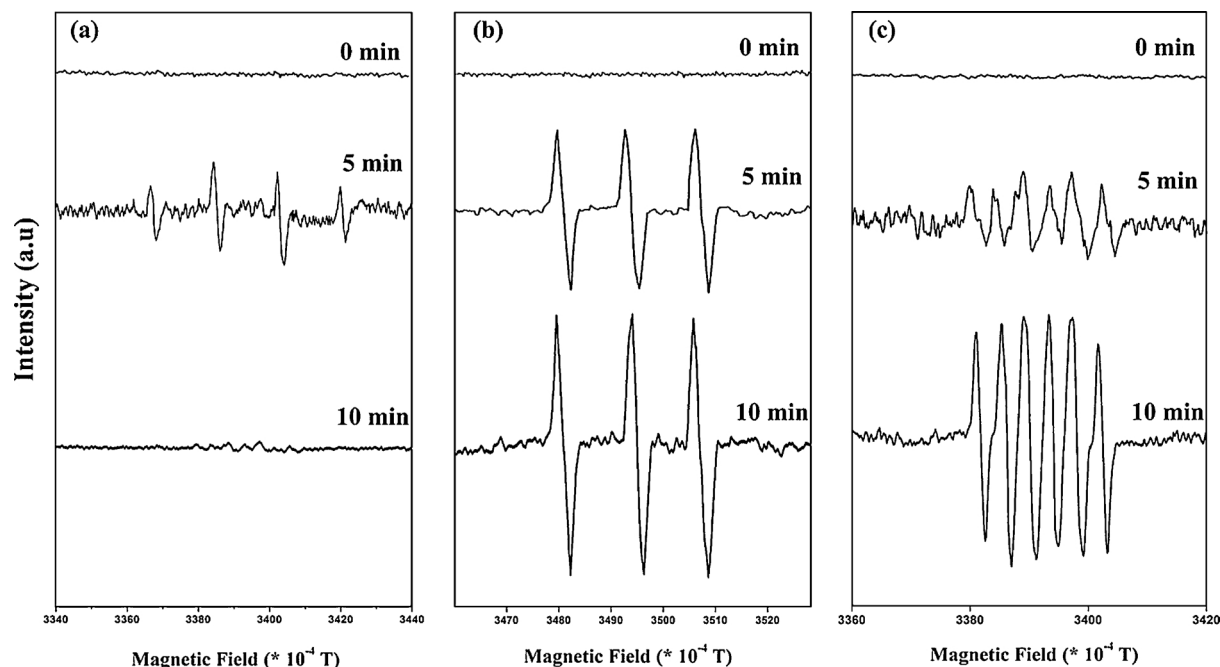


Fig. 10. ESR spectra of (a) hydroxyl radicals species trapped by DMPO, (b) singlet oxygen species trapped by TEMP, (c) superoxide radical species trapped by DMPO/DMSO.

radical was more dominant.

The HRTEM (Fig. 11(a)) showed the formation of the vacancies in the Fe@3D-WS₂, which could act as the free carriers of electrons and holes. The possible formation path of the vacancies was showed in Fig. 11(b). As assumed in recent study, the polarization pointed from S vacancies to W vacancies was along with the armchair direction [9]. A piezoelectric polarization could be generated from the armchair direction when a mechanical force was applied on the Fe@3D-WS₂ surface. Fig. 11(c) displayed the formation mechanism of the free radicals. When a ball milling activation was applied on the Fe@3D-WS₂ surface, a piezoelectric potential could be generated from the active edge sites of Fe@3D-WS₂ by following reaction. Firstly, positive charges were accumulated on one side of Fe@3D-WS₂ surface by internal polarization due to the transport of the electrons to the left-hand side. Similarly, negative charges were accumulated on the other side of Fe@3D-WS₂ surface by the right-side transformation of the holes (see Eq. (2)) [10]. Then, ·OH radicals were generated by the reaction of the water molecule and the surface positive charges (see Eq. (2)) [44]. On the right hand, the ¹O₂ radicals were generated by the reaction of surface negative charges with O₂ (see Eq. (3)) [45]. Finally, LEVO was

decomposed into small molecule compounds, CO₂, NO₃[−] and F[−] by the generated ·OH radicals and oxygen radicals.



4. Conclusions

In summary, the few-layer 3D-WS₂ with abundant active edges and vacancies was successfully synthesized via a simple ball milling method. The single-layer of the as-prepared Fe@3D-WS₂ provided more 1 T phase, which was beneficial for piezo-degradation of LEVO under ball milling treatment. The DFT calculations demonstrated that the loaded Fe atoms could increase the length of nearest W–S bonds and decrease the band gap width of WS₂. As a result, the piezo-degradation activity was significantly improved by the increasing of the non-centrosymmetric property and the reducing of the separation resistance of the electron and hole. Cyclic tests confirmed that the excellent

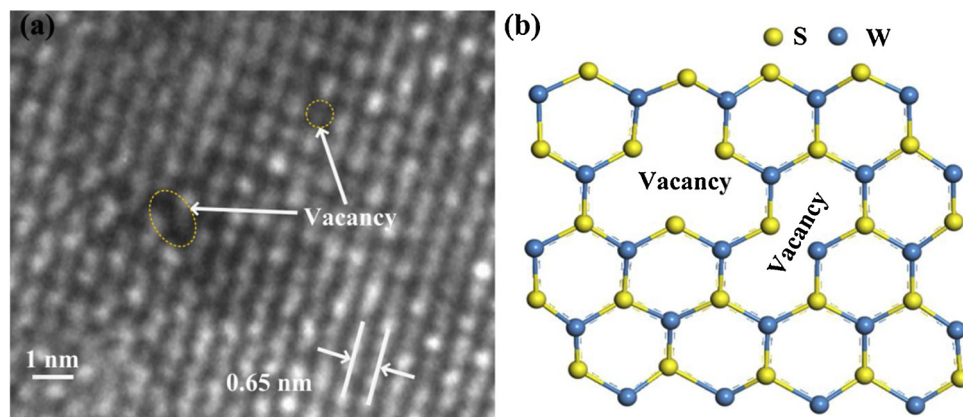


Fig. 11. Piezo-catalytic degradation mechanism of LEVO by Fe@3D-WS₂. (a) HRTEM image of the Fe@3D-WS₂ with vacancies. (b) Atomic structure of Fe@3D-WS₂ with vacancies. (c) The generation mechanism of free radicals by Fe@3D-WS₂ under ball milling activation.

reusability of the Fe@3D-WS₂ mainly attributed to its “self-renewing” behavior, as the new single-layer active edges were continually generated. Furthermore, the radical quenching results and ESR spectra demonstrated that both oxygen radicals and hydroxyl (OH[·]) radicals were generated and took part in the LEVO degradation, in which the contribution of ¹O₂ radicals was more dominant. This work creates a new method for efficient degradation of organics by trigger piezoelectric catalysis via ball-milling.

Acknowledgements

The authors acknowledge funding support from the National Natural Science Foundation of China (21677027), the Fundamental Research Funding for the Central Universities (DUT17ZD225) and NSFC-Xinjiang Unite Funding (U1403194) are gratefully acknowledged.

Appendix A. Supplementary data

Supplementary material related to this article can be found, in the online version, at doi:<https://doi.org/10.1016/j.apcatb.2019.04.020>.

References

- [1] M.J. Wu, T. Zheng, H.W. Zheng, J.F. Li, W.H. Wang, M.S. Zhu, F.Z. Li, G.T. Yue, Y.Z. Gu, J.G. Wu, *J. Mater. Chem. A* 6 (2018) 16439–16449.
- [2] X.Q. Fang, J.X. Liu, V. Gupta, *Nanoscale* 5 (2013) 1716–1726.
- [3] Y. Su, L. Zhang, W.Z. Wang, X.M. Li, Y.L. Zhang, D.K. Shao, *J. Mater. Chem. A* 6 (2018) 11909–11915.
- [4] C. Liu, A. Yu, M. Peng, M. Song, W. Liu, Y. Zhang, J. Zhai, *J. Phys. Chem. C* 120 (2016) 6971–6977.
- [5] C. Liu, M. Peng, A. Yu, J. Liu, M. Song, Y. Zhang, J. Zhai, *Nano Energy* 26 (2016) 417–424.
- [6] S. Manzeli, D. Ovchinnikov, D. Pasquier, O.V. Yazyev, A. Kis, *Nature* 17033 (2017) 1–15.
- [7] S.Y. Lan, J.X. Feng, Y. Xiong, S.H. Tian, S.W. Liu, L.J. Kong, *Environ. Sci. Technol.* 51 (2017) 6560–6569.
- [8] J.M. Wu, W.E. Chang, Y.T. Chang, C.K. Chang, *Adv. Mater.* 28 (2016) 3718–3725.
- [9] J.H. Lin, Y.H. Tao, M.H. Wu, T.M. Chou, Z.H. Lin, J.M. Wu, *Nano Energy* 31 (2017) 575–581.
- [10] S. Masimukku, Y.C. Hu, Z.H. Lin, S.W. Chan, T.M. Chou, J.M. Wu, *Nano Energy* 46 (2018) 338–346.
- [11] S. Romeis, J. Schmidt, W. Peukert, *Int. J. Miner. Process.* 156 (2016) 24–31.
- [12] F. Stenger, S. Mende, J. Schwedes, W. Peukert, *Chem. Eng. Sci.* 60 (2005) 4557–4565.
- [13] A.K. Giri, *Adv. Mater.* 9 (1991) 163–167.
- [14] J.T. Xu, I. Jeon, J. Seo, S.X. Dou, L.M. Dai, J. Baek, *Adv. Mater.* 26 (2014) 7317–7323.
- [15] X.M. Zhou, N. Liu, J. Schmidt, A. Kahnt, A. Osvet, S. Romeis, E.M. Zolnhofer, V.R.R. Marthala, D.M. Guldin, W. Peukert, M. Hartmann, K. Meyer, P. Schmuki, *Adv. Mater.* 29 (2017) 1604747–1604754.
- [16] I. Jeon, H. Choi, S. Jung, J. Seo, M. Kim, L.M. Dai, J. Baek, *J. Am. Chem. Soc.* 135 (2013) 1386–1393.
- [17] Y. Zhang, Y. Liu, Z.L. Wang, *Adv. Mater.* 23 (2011) 3004–3013.
- [18] X. Xue, W. Zang, P. Deng, Q. Wang, L. Xing, Y. Zhang, Z. Wang, *Nano Energy* 13 (2015) 414–422.
- [19] A. Molinari, E. Sarti, N. Marchetti, L. Pasti, *Appl. Catal. B: Environ.* 23 (2017) 9–17.
- [20] I. Epold, M. Trapido, N. Dulova, *Chem. Eng. J.* 279 (2015) 452–462.
- [21] B. Yan, C.H. Niu, J. Wang, *Environ. Sci. Technol.* 51 (2017) 8048–8056.
- [22] M.F. Nazar, M.A. Saleem, S.N. Bajwa, B. Yameen, M. Ashfaq, M.N. Zafar, M. Zubair, *J. Phys. Chem. B* 121 (2017) 437–443.
- [23] I. Sousa, V. Claro, J.L. Pereira, A.L. Amaral, L. Cunha-Silva, B.D. Castro, M.J. Feio, E. Pereira, P. Gameiro, *J. Inorg. Biochem.* 110 (2012) 64–71.
- [24] F.C. Moreira, R.A.R. Boaventura, E. Brillas, V.J.P. Vilar, *Appl. Catal. B: Environ.* 202 (2017) 217–261.
- [25] D. Ding, C. Liu, Y. Ji, Q. Yang, L. Chen, C. Jiang, T. Cai, *Chem. Eng.* 308 (2017) 330–339.
- [26] A. Manikandan, P.R. Liango, C.W. Chen, Y.C. Wang, Y.C. Shih, L. Lee, Z.M. Wang, H. Ko, Y. Chueh, *J. Mater. Chem. A* 6 (2018) 15320–15329.
- [27] M.A. Lukowski, A.S. Daniel, F. Meng, A. Forticaux, L. Li, S. Jin, *J. Am. Chem. Soc.* 135 (2013) 10274–10277.
- [28] L. Yang, X.D. Cui, J.Y. Zhang, K. Wang, M. Shen, S.S. Zeng, S.A. Dayeh, L. Feng, B. Xiang, *Sci. Rep.* 4 (2014) 5649–5658.
- [29] K.S. Liang, R.R. Chianelli, F.Z. Chien, S.C. Moss, *J. NonCryst. Solids* 79 (1986) 251–273.
- [30] M. Chhowall, G.A. Amarantung, *J. Nature* 407 (2000) 164–167.
- [31] C. Lee, H. Yan, L.E. Brus, T.F. Heinz, J. Hone, S. Ryu, *ACS Nano* 4 (2010) 2695–2700.
- [32] A. Berkdemir, H.R. Gutiérrez, A.R. Botello-Méndez, N. Perea-López, A.L. Elías, C.I. Chia, B. Wang, V.H. Crespi, F. López-Urías, J.C. Charlier, H. Terrones, M. Terrones, *Sci. Rep. UK*, 3 (2013) 1755–1763.
- [33] Y. Zhang, Y. Zhang, Q. Ji, J. Ju, H. Yuan, J. Shi, T. Gao, D. Ma, M. Liu, Y. Chen, X. Song, H.Y. Wang, Y. Cui, Z. Liu, *ACS Nano* 7 (2013) 8963–8971.
- [34] C.C. Mayorga-Martínez, A. Ambrosi, A.Y.S. Eng, Z. Sofer, M. Pumera, *Adv. Funct. Mater.* 25 (2015) 5611–5616.
- [35] D. Voiry, H. Yamaguchi, J. Li, R. Silva, D.C.B. Alves, T. Fujita, M. Chen, T. Asefa, V.B. Shenoy, G. Eda, M. Chhowall, *Nat. Mater.* 12 (2013) 850–855.
- [36] M.H. Zhao, Z.L. Wang, S.X. Mao, *Nano Lett.* 4 (2004) 587–590.
- [37] H. Liu, N. Han, J. Zhao, *RSC Adv.* 5 (2015) 17572–17581.
- [38] S. Haldar, H. Vovusha, M.K. Yadav, O. Eriksson, B. Sanyal, *Phys. Rev. B* 92 (2015) 235408–235414.
- [39] X.J. Wen, C.G. Niu, H. Guo, L. Zhang, C. Liang, G.M. Zeng, *J. Catal.* 358 (2018) 211–223.
- [40] M.S. Yahya, M.E. Karbane, N. Oturan, K.E. Kacemi, M.A. Oturan, *Environ. Technol.* 37 (2016) 1276–1287.
- [41] G.V. Buxton, *J. Phys. Chem. Ref. Data* 17 (1988) 513–886.
- [42] L. Zhou, M. Sleiman, C. Ferronato, J.M. Chovelon, P. de Sainte-Claire, C. Richard, *Water Res.* 123 (2017) 715–723.
- [43] Y. Wang, H. Sun, H.M. Ang, M.O. Tadé, S. Wang, *Appl. Catal. B: Environ.* 164 (2015) 159–167.
- [44] Z. Zhang, J.T. Yates, *Chem. Rev.* 112 (2012) 5520–5551.
- [45] Z. Zhang, J.T. Yates, *J. Phys. Chem. Lett.* 1 (2010) 2185–2188.